Polym. Korea, Vol. 47, No. 5, pp. 678-685 (2023)
https://doi.org/10.7317/pk.2023.47.5.678

ISSN 0379-153X(Print)
ISSN 2234-8077(Online)

조직 유사 팬텀의 근적외선 투과 깊이에 따른 유기 및 무기 물질 광열 효율 평가

황주영 · 림 므함디 · 반유 피르다우스 수리야위자야 · 김민찬* · 아스트리니 프라디야스티** · 충탄팜 · 현 규*
김현중*** · 이송이 · 김문호** · 곽민석†

부경대학교 화학과 4차산업융합바이오닉스공학과, *부산대학교 화공생명공학부
**부경대학교 고분자공학과, ***미국 클리블랜드 클리닉

(2023년 7월 4일 접수, 2023년 7월 21일 수정, 2023년 7월 21일 채택)

Assessment of Near-infrared Penetration Depth and Photothermal Efficiency of Organic and Inorganic Materials in Tissue-mimicking Phantoms

Juyoung Hwang, Rim Mhamdi, Banyu Firdaus Soeriawidjaja, Min Chan Kim*, Astrini Pradyasti, Chung Thanh Pham, Kyu Hyun*, Hyun Jung Kim***, Songyi Lee, Mun Ho Kim**, and Minseok Kwak†**

Department of Chemistry and Industry 4.0 Convergence Bionics Engineering, Pukyong National University
**School of Chemical Engineering, Pusan National University, 2 Busandaehak-ro 63 beon-gil, Geumjeong-gu, Busan 46241, Korea*
***Department of Polymer Engineering, Pukyong National University, 45 Yongso-ro, Nam-gu, Busan 48513, Korea*
****Department of Inflammation and Immunity, Lerner Research Institute, Cleveland Clinic, 9500 Euclid Ave., NE3, Cleveland, OH, 44195, USA*

(Received July 4, 2023; Revised July 21, 2023; Accepted July 21, 2023)

초록: 본 연구는 피부조직을 모방한 아크릴아마이드 기반 팬텀을 사용하여 광열치료에서 근적외선 빛이 얼마나 깊이 투과하는지를 평가하였다. 인도시아닌그린, IR788, PA2, 금 나노 막대와 같은 다양한 광열제를 팬텀에 첨가하였다. 근적외선 레이저 조사하에서 광열제의 온도 변화를 다양한 팬텀 뚜껑의 높이에 따라 측정하였으며, 이에 따라 온도 감소는 뚜껑의 두께와 비례한다는 결과를 얻었다. 또한 온도변화와 투과율이 직접적으로 관련이 있었으며, Pearson 상관계수 또한 높은 값을 가졌다. 광열제의 광열 전환 효율을 계산하였고, 그 중 금 나노 막대가 팬텀에서 근적외선 레이저 조사로부터 가장 에너지 흡수율이 높았다. 이 결과로부터 아크릴아마이드 기반 팬텀은 조직 조건하에서의 광열치료에서 광열제의 성능을 연구하기 위한 중요한 플랫폼을 제공할 수 있을 것이라 기대한다.

Abstract: This study evaluated how deeply near-infrared light (NIR) can penetrate skin tissue in photothermal therapy (PTT) using an acrylamide-based phantom that mimics skin tissue. We loaded the phantom with varied photothermal agents (PTAs) such as indocyanine green (ICG), IR788, PA2, and gold nanorod (AuNR). The temperature change of the PTAs under a NIR laser irradiation was assessed at different phantom lid thicknesses, resulting in temperature drop is proportional to lid-thickness. Moreover, Pearson's correlation coefficient indicated that the temperature change and transmittance were directly related, having high values. The trends observed in the study were consistent with the respective photothermal conversion efficiency values of the PTAs. The results suggest that AuNR is superior to ICG and IR788-sIPN as a PTA for absorbing energy from laser irradiation in the phantom. The acrylamide-based phantom provides a valuable platform for further research into the performance of PTAs for PTT under tissue conditions.

Keywords: phantom, photothermal therapy, near-infrared, indocyanine green, gold nanorod.

Introduction

Photothermal therapy (PTT), which involves the energy conversion of near-infrared (NIR) electromagnetic wave into heat, can induce local tumor ablation through hyperthermia phenomena.[1,2] This method has been observed to bring about tumor cell death by destroying the cell membrane and denaturing proteins.[3,4] Maintaining hyperthermia, which involves raising the temperature of the tumor site to over 50 ℃, has been shown to promote these effects.[5,6] PTT offers a distinct advantage over other therapeutic methods, such as surgery,

†To whom correspondence should be addressed.
mkwak@pukyong.ac.kr, ORCID 0000-0002-0480-1804

chemotherapy, and radiotherapy, as it allows for the localized exposure of a tumor area under an NIR laser, thereby reducing side effects.[7-9] More often, PTT can be used for the treatment of skin cancer, including melanoma and carcinoma.[10] However, its efficacy is limited when dealing with tumors deeply located beneath skin tissue due to the significant weakening of NIR light penetration caused by hemoglobin, water, and melanin.[11,12] Moreover, the effective penetration depth of PTT is restricted to only few millimeters under the surface of the skin tissue owing to scattering by substances within the skin tissue.[13] Therefore, it is necessary to develop tissue-like phantoms to establish and refine quantitative details prior to *in vivo* testing or clinical trials.

Photothermal agents (PTAs) are used to mediate PTT for the thermal ablation of cancer, and can be classified into two categories: organic and inorganic materials.[14] Examples of organic PTAs include indocyanine green (ICG) and IR780.[15] In contrast, inorganic PTAs include gold nanorods (AuNRs), silver nanoparticles, and carbon nanotubes, which exhibit strong absorption of NIR light corresponding to NIR laser irradiation.[16-18] However, the use of organic and inorganic compounds as PTAs is limited by their poor water solubility and rapid elimination from the body.[19] To overcome these limitations, it is necessary to encapsulate the PTAs inside nanoparticles to improve their solubility and stability.[20-22]

Tissue-like phantoms are a valuable tool for predicting the thermal response of tissue upon exposure to NIR laser, as they offer a means to understand the propagation and absorption of light and subsequent rise in tissue temperature.[23] Liquid tissue-like phantoms are widely used for this purpose, as they are flexible, easy to fabricate and offer adjustable optical properties by controlling the mixing ratio of the absorber (*e.g.*, India ink, Evans blue, and Naphthol Green) and scattering agent (*e.g.*, Intralipid, Liposyn, and polystyrene microspheres) in the phantom solution.[24-26]

Although various materials have been used to prepare phantoms that mimic the scattering properties of biological tissue, Intralipids have been frequently used due to their ease of handling and low cost.[27] Polyacrylamide-based phantoms are stable at 60 ℃ and transparent in the NIR region.[28,29] These phantoms can also be mixed with Intralipid to achieve the desired optical properties.[30] Furthermore, Intralipids are turbid and have no strong absorption at visible wavelengths, making them well-characterized and extensively studied.[31,32] Therefore, acrylamide-based phantoms with Intralipid have scattering coefficients similar to those of biological tissue in the NIR and are thus primarily used as tissue-mimicking phantom media.

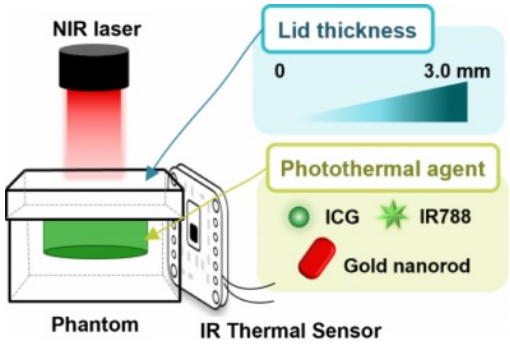

Scheme 1. Schematic illustration for measurement of near-infrared (NIR) penetration depth and photothermal efficiency of photothermal agents using an IR thermal sensor in tissue-mimicking phantoms.

To achieve successful PTT using PTAs, it is crucial to consider the transmittance and temperature control from the skin surface to the deep tissue when exposed to a NIR laser. Therefore, it is essential to study the correlation between the transmittance of near-infrared wavelengths and temperature in a turbid medium exposed to NIR lasers. By understanding the relationship between tissue's optical properties and light energy distribution, the temperature distribution can be predicted, which is critical for effective PTT.[33] In particular, the temperature rise must be tightly controlled, as excessive heating can lead to tissue damage or destruction.[34] Therefore, studies that investigate the correlation between the optical properties of tissue and temperature distribution in a turbid medium are crucial for safe and effective PTT.

In this study, we developed a skin tissue-mimetic phantom using several PTAs that were loaded and covered with lids ranging in thickness from 0 to 3.0 mm. The tissue-like phantom was fabricated with viscoelastic properties comparable to those of human skin, making it a suitable platform for determining the depth of NIR light penetration in PTT (Scheme 1). Performance of mostly used PTAs within the platform was then evaluated with experimental data and statistics, which further lead to the creation of a temperature prediction system. Our findings demonstrate the significance of utilizing a tissue-like phantom to assess the effectiveness of PTAs and offer a valuable tool for determining the optimal PTA to use in PTT.

Experimental

Materials and Methods. Reagents: *N*,*N*,*N*′,*N*′-tetramethylethylenediamine (TEMED, 99.0%), Intralipid (20% emulsion),

ammonium persulfate (APS), Pluronic F127 (M_n 12600), and pentaerythritol tetraacrylate (PETA) were obtained from Sigma Aldrich (MO, USA), while acrylamide/bis-acrylamide solution (AM solution, 19:1, 30%) was acquired from BioRad (CA, USA). ICG was purchased from Tokyo Chemical Industry (Tokyo, Japan), and Lumogen® IR788 was generously offered by BASF AG (Germany). All aqueous solutions were purified using ultra-pure deionized water (DW) obtained from a Millipore system (≥18 MΩ, Milli-Q, Millipore, Germany).

Fabrication of Phantom. The fabrication of acrylamide phantom followed the method described with a slight modification in composition and scale.[26] To prepare the pre-gel solution, Intralipid-10% (0.66 mL), 10% APS (0.098 mL), DW (7.2 mL), and TEMED (0.068 mL) were added to the AM solution (7.0 mL). The resulting mixture was gently vortexed and poured into a well template, allowing it to gel for 2 h. Upon its removal from the mold, the phantom was washed with DW and then four PTAs were separately loaded into the wells. The lids varying in six thickness was fabricated using the same method with spacers and glass plates.

Preparation of Photothermal Agents. AuNR and PA2 were synthesized using previously reported methods.[35,36] The IR788-sIPNs and PA2-sIPNs were prepared following the protocol described in our published reports.[21,22] In brief, F127 (0.5 g) and IR788 or PA2 (3 wt% ratios of F127) were dissolved in chloroform in a glass vial, and PETA (2.5 wt% ratios of F127) was dissolved in chloroform in a separate glass vial. After complete evaporation of organic solvents using a rotary evaporator, an F127-dye film, and a PETA film were obtained. The F127-dye film was hydrated by adding 4.5 mL of DW to the vial, followed by stirring at 24 ℃ using an orbital shaker (200 rpm, 12 h). The F127-dye solution was then transferred to the PETA-filmed vial and stirred for another 12 h. The vial was filled with argon gas and heated at 60 ℃ for 10 min. Subsequently, a cover glass was placed over the vial, which was exposed to UV radiation from a Lumen Dynamic Omnicure series 200 UV lamp with a 320-500 nm filter at a power of 1.5 W/cm^2 at 50 ℃ for 6 min to crosslink the F127 micelle core. Finally, the UV-exposed solution was slowly cooled down at 24 ℃ and filtered using a 0.2 μm Minister® syringe filter (Sartorius Stedim, France) to remove residual PETA and free dyes.

Viscoelasticity Characterization of Phantom. The rheological properties were measured using an ARES-G2 rheometer (TA Instruments, USA) with a 25 mm stainless-steel parallel-plate geometry and advanced Peltier system for controlled temperature. To prevent the slip during the test, sample was loaded as solution and then the sample became gel in the geometry. Strain sweep test was carried out to check the linear viscoelastic (LVE) regime at a frequency of 1 rad/s and temperature of 25 ℃. Frequency sweep test was carried out at a fixed strain amplitude of 0.005 (0.5%) within LVE regime and temperature of 25 ℃, and frequencies from 0.1 to 100 rad/s. The transmittance and absorption spectra were measured using a spectramax M2 spectrophotometer (Molecular Devices, CA, USA).

Temperature Measurement in Phantom Gels Under NIR Laser Irradiation. To evaluate the photothermal effect of ICG, IR788-sIPN, and AuNR, the substances were diluted to appropriate concentrations to achieve a maximum temperature of 60 ℃ upon exposure to an 808 nm laser (Changchun New Industries Optoelectronics Technology Co., Ltd. Jilin, China) at a power density of 1.5 W/cm^2 for 5 min. Subsequently, 100 μL of a 2 mg/mL ICG solution, 3% IR788-sIPN (diluted 2-fold), and AuNR were added to the phantom well and exposed to an 808 nm laser (1.5 W/cm^2, 5 min). During this process, temperature changes were monitored every 5 s using a previously reported AMG8833 device.[37]

Results and Discussion

Characterization of Acrylamide-Based Phantom. The rheological properties of the acrylamide-based phantom were evaluated to determine its similarity to human skin tissue. From frequency sweep test, the storage modulus (G') of the phantom gels show plateau and are much larger than loss modulus (G'') at entire frequency range (see Figure 1(a)). The G'' are not measured due to too low a value at low frequency ranges). As results, tan δ ($\equiv G''/G'$) was very low value ($<<10^{-2}$). This frequency independence of storage modulus and low tan δ value indicate that the phantom gel is elastic materials like rubber or elastomer. The storage modulus of the phantom was measured at different angular frequencies. The storage modulus of the phantom was found to be 52.2 kPa, which is comparable to the measured value of 56 kPa for human dermis in skin tissue (7% error rate). These findings indicate that the phantom closely mimics the physical properties of human skin tissue, which is vital for accurately assessing the effectiveness of PTT.

Figure 1(b) shows the optical characteristics of the phantom lid with varying thicknesses. The transmittance of visible-near infrared (vis-NIR) light within the wavelength range of 400-900 nm was observed to vary in relation to the thickness of the lid. The 808 nm wavelength laser is widely utilized in

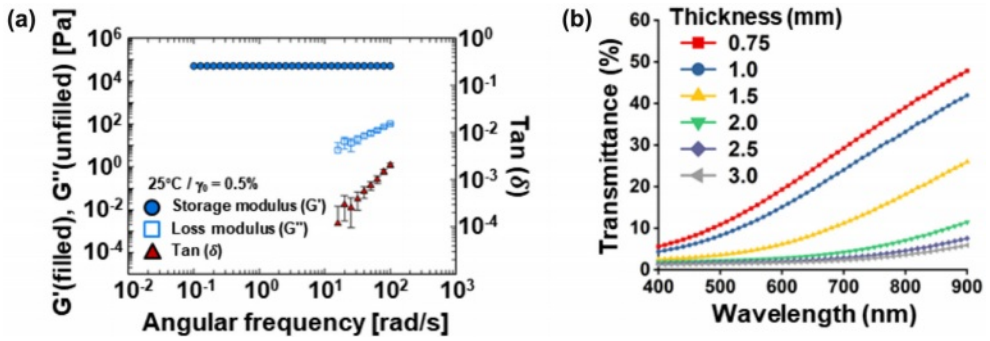

Figure 1. Physical properties of acrylamide-based phantom: (a) storage modulus (G'), loss modulus (G''), and tan (δ) value of phantom as a function of frequency; (b) Visible-near infrared (vis-NIR) transmittance spectra at various thickness of phantom lid (0.75, 1.0, 1.5, 2.0, 2.5, and 3.0 mm, respectively).

PTT due to its favorable properties. It is worth noting that the mean transmittance at 808 nm decreases with an increase in lid thickness. Specifically, at a lid thickness of 0.75 mm, the mean transmittance reduces to 39.05%, while at a lid thickness of 2 mm, the mean transmittance is less than 10% (Figure S1). These results indicate that the lid thickness has a significant effect on the penetration of NIR light and could affect the photothermal conversion efficiency (PCE) of PTAs in the phantom.

Optical Properties of Photothermal Agents. The optical properties of organic and inorganic PTAs were first evaluated. ICG (Figure 2(a)), IR788 (Figure 2(b)), and PA2 (Figure 2(c)) are organic photothermal materials that belong to the class of heptamethine cyanine dyes, while $44.9 \pm 10 \times 10 \pm 1.6$ nm (length × width) AuNR (Figure S2) is an inorganic photothermal material that is also widely used in various applications.[38,39] IR788 and PA2 were loaded into F127-sIPN owing to poor solubility in aqueous solution, while ICG and AuNR showed good dispersity in water. Then we analyzed the absorbance of PTAs using a Vis-NIR spectrophotometer (Figure 2(d)). ICG, IR788-sIPN, and AuNR show strong absorption in the NIR range of 750-900 nm. Interestingly, it was observed that the absorption spectrum of PA2, following its loading into F127-sIPN to enhance its aqueous solubility, exhibited a blue shift, and the marked absorption band around 808 nm was absent. Consequently, ICG, IR788-sIPN, and AuNR remarkably increase optical absorption in the NIR region, which proves the role of photothermal agents for NIR-induced photothermal therapy.

Temperature Changes Under Exposed NIR Laser. Following confirmation of the strong absorption of the PTAs at around 800 nm, we proceeded to investigate their photothermal effect under subsequent 808 nm laser irradiation at a power density of 1.5 W/cm^2 for a duration of 300 s. The NIR laser was pointed to the phantom, which was positioned at a distance of 10 mm within a well size of 7 mm. Temperature changes were monitored on the side of the phantom using an IR-sensored device for continuous temperature recording (Fig-

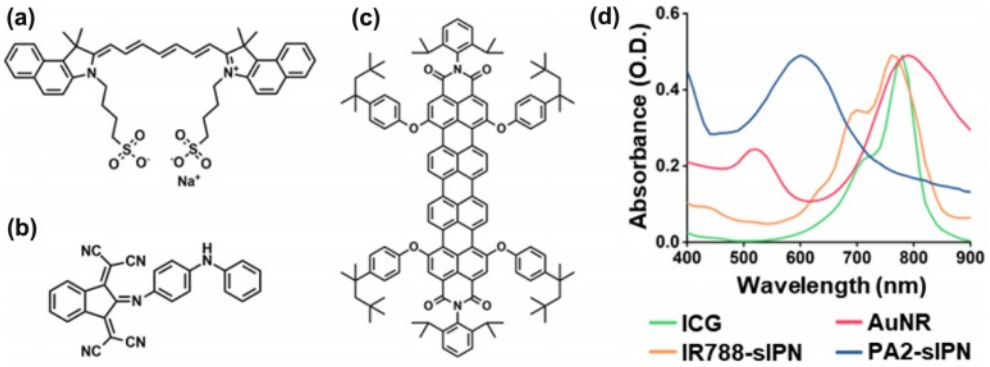

Figure 2. Chemical structure of (a) ICG; (b) PA2; (c) IR788; (d) Vis-NIR absorbance spectra of ICG, IR788-sIPN, AuNR, and PA2-sIPN solutions.

ure S3). ICG, IR788-sIPN, and AuNR exhibited a rapid temperature increase until 100 s, with the maximum temperature being reached at approximately 300 s under 808 nm laser irradiation (Figure S4). Under 808 nm laser irradiation for a duration of 300 s, ICG, IR788-sIPN, and AuNR achieved their maximum temperatures of approximately 60 ℃, while water heated to 39.9 ℃ (Figure S5). We also investigated the effect of lid thickness on the temperature changes, with a linear decrease observed as the thickness of the lid increased (Figure S6). Notably, when the thickness of the lid reached 3.0 mm, the highest temperatures attained by ICG, IR788-sIPN, and AuNR were 44.2, 40.2, and 42.0 ℃, respectively, which closely approximates the temperature of water at 39 ℃ (Figure S7A). This could be attributed to the NIR light exhibited a substantial degree of scattering at this thickness. Consequently, a significant reduction in transmittance occurred, impeding any further increase in temperature. We also evaluated whether PA2-sIPN could raise the temperature under NIR laser exposure, despite its low absorption at 808 nm. However, the temperature of PA2-sIPN under NIR laser irradiation did not rise significantly, remaining at 37.80 ℃, which is similar to that of water (Figure S7(a) and (b)). Thus, ICG, IR788-sIPN, and AuNR can be heated up to above 50 ℃, the temperature required for PTT under NIR laser, in the skin tissue-mimetic phantom with lid thickness of up to 1.5 mm (Figure 3(a) to (c)).

Correlation Between Transmittance and Temperature. To assess the impact of the acrylamide phantom gel platform on the performance of PTAs, we conducted a comparison of the phantom's transmittance at 808 nm wavelength and the temperature change of the PTAs at different lid thicknesses. These values were expressed as percentages, with a maximum value of 100% represents the phantom's transmittance and the temperature change of the PTAs at a thickness of 0 mm (without lid). The latter expressed using the variable $\%\Delta T$, which is defined as:

$$\%\Delta T = \frac{T^{d}_{max} - T^{d}_{start}}{T^{0}_{max} - T^{0}_{start}} \times 100\% \quad (1)$$

Where T^{d}_{max} and T^{d}_{start} represent the maximum temperature of PTA and starting temperature of PTA during irradiation at a lid thickness of d, respectively, while T^{0} the maximum or starting temperature of PTA at a lid thickness of 0 mm. We used this variable to calculate the Pearson correlation coefficient (r) for each PTA in order to quantify the relationship between temperature change and transmittance at various lid thicknesses, as shown in the following equation:

$$r = \frac{\sum(\%\Delta T_i - \overline{\%\Delta T})(\%Transm_i - \overline{\%Transm})}{\sqrt{\sum(\%\Delta T_i - \overline{\%\Delta T})^2 (\%Transm_i - \overline{\%Transm})^2}} \quad (2)$$

Here, the subscript i denote individual sample points, while the variable with a bar accents represents the sample mean. Table 1 shows that all PTAs had a correlation coefficient of >0.89, indicating a strong direct relationship between temperature change and transmittance. Among the PTAs tested, IR788-sIPN exhibited the highest correlation coefficient, which

Table 1. Correlation Coefficient, Linear Fitting Parameter Values, and Lid Thickness for 50 ℃ of Each PTA

Contents	r	Slope (a)	Intercept (b)	Lid[a] (mm)
ΔT ICG	0.89	-0.0783	8.184	2.1
ΔT IR788-sIPN	0.98	-0.0637	6.355	1.7
ΔT AuNR	0.93	-0.0820	7.868	1.9

[a]Thickness values reaching 50 ℃ for each PTA were calculated by fitting the experimental data.

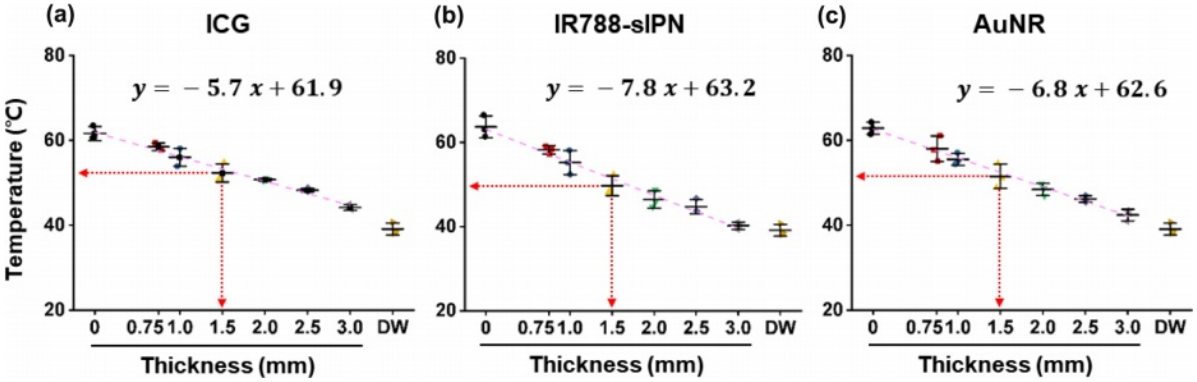

Figure 3. The temperature of (a) ICG; (b) IR788-sIPN; (c) AuNR with different thickness of the lid under 808 nm laser irradiation at 300 s.

was the closest to 1, indicating that IR788-sIPN behaves similarly to transmittance in the phantom platform and has almost the same rate of a temperature change.

To further investigate the behavior of %transmittance and %Δ*T* in a phantom system with increasing lid thickness, we created Figure S8 and S9. Interestingly, both parameters exhibit a negative correlation with the thickness of the lid. This suggests that a thicker lid hinders the penetration of the light source, thereby reducing the amount of transmitted and absorbed light by the PTA, leading to the lower temperatures. These findings are consistent with the PCE values of each PTA (Table S1). It is important to note that for %Δ*T*, since the mathematical model used to compare the results takes into account the presence of the lid, Figure S9 starts at a thickness of 0.75 mm.

In this acrylamide phantom platform, we found out that lid thickness exhibits an exponential relation with %transmittance, while %Δ*T*, for all PTAs has a linear relationship with lid thickness. By fitting equations to both graphs (see supplementary information for detailed formulation), we can express the relationship between temperature change and transmittance suing following equation:

$$\%\Delta T = \frac{3.17(e^{-0.05\times\%Trans}) - b_{PTA}}{a_{PTA}} \quad (3)$$

With a_{PTA} and b_{PTA} represent the slope and intercept of each PTA, respectively, and can be found in Table 1. The equation shows that %transmittance and %Δ*T* are related exponentially, allowing for the prediction of how the temperature of a PTA would behave against transmittance within an acrylamide phantom platform with varying lid thickness under 808 nm laser irradiation. Higher values of a_{PTA} and b_{PTA} lead to higher %Δ*T*, indicating that PTAs will lose less heat as the lid thickens, compared to PTAs with lower a_{PTA} and b_{PTA} values. An excel file containing this prediction system is available in supplementary information for quick estimation in terms of PTAs, initial temperature, and penetration depth.

Conclusions

In conclusion, acrylamide-based phantoms that mimic the viscoelasticity and optical property of skin tissue are effective tools for studying the penetration depth of NIR light in PTT. Since the phantom contains an opaque Intralipid, the thickness of the lid affects the transmittance of NIR light, with the quantity of transmittance decreasing as the lid thickness increases. By appropriately diluting organic (ICG, IR788, PA2) or inorganic (AuNR) PTAs, we were able to achieve the initial temperature of 60 ℃ upon exposure to an NIR laser, allowing us to evaluate the temperature change caused by varying lid thickness. Our results demonstrate that these PTAs can attain temperatures above 50 ℃, which is the minimum threshold required for effective PTT, in skin tissue-mimicking phantoms with lid thicknesses of up to 1.5 mm. Moreover, our data reveal a direct exponential relationship between the temperature change of PTA and transmitted light, as proven by high value of Pearson's correlation coefficient (> 0.89) and rearrangement of fitting model equations. Overall, our findings provide valuable insights into how popular PTAs behave in tissue-like phantoms, which may ultimately enable the development of more potent PTT for various therapeutic applications.

Acknowledgments: We thank Joo H. Kang at Ulsan National Institute of Science and Technology for fabrication of PTFE mold for phantom. This research was supported by the programs through the National Research Foundation of Korea (NRF) funded by the Ministry of Science and ICT (NRF-2020R1A2C1010766 and NRF-2022R1A5A8023404).

Conflict of Interest: The authors declare that there is no conflict of interest.

Supporting information: Information is available regarding the characterization of phantom and gold nanorod, temperature changes of PTAs under an NIR laser exposure, Photothermal conversion efficiency value references for the PTAs, and Step-by-step derivation of %transmittance vs. %Δ*T* equation. The materials are available *via* the Internet at http://journal.polymer-korea.or.kr.

References

1. Wang, P.; Chen, B.; Zhan, Y.; Wang, L.; Luo, J.; Xu, J.; Zhan, L.; Li, Z.; Liu, Y.; Wei, J. Enhancing the Efficiency of Mild-Temperature Photothermal Therapy for Cancer Assisting with Various Strategies. *Pharmaceutics* **2022**, 14, 2279.
2. Shi, X.; Tian, Y.; Liu, Y.; Xiong, Z.; Zhai, S.; Chu, S.; Gao, F. Research Progress of Photothermal Nanomaterials in Multimodal Tumor Therapy. *Front. Oncol.* **2022**, 12, 939365.
3. Gao, J.; Wang, W. Q.; Pei, Q.; Lord, M. S.; Yu, H. J. Engineering Nanomedicines Through Boosting Immunogenic Cell Death for Improved Cancer Immunotherapy. *Acta. Pharmacol. Sin.* **2020**, 41, 986-994.

4. Tranberg, K. G. Local Destruction of Tumors and Systemic Immune Effects. *Front. Oncol.* **2021**, 11, 708810.
5. Xia, Q. S.; Liu, X.; Xu, B.; Zhao, T. D.; Li, H. Y.; Chen, Z. H.; Xiang, Q.; Geng, C. Y.; Pan, L.; Hu, R. L.; Qi, Y. J.; Sun, G. F.; Tang, J. T. Feasibility Study of High-temperature Thermoseed Inductive Hyperthermia in Melanoma Treatment. *Oncol. Rep.* **2011**, 25, 953-62.
6. Itoh, Y.; Yamada, Y.; Kazaoka, Y.; Ishiguchi, T.; Honda, N. Combination of Chemotherapy and Mild Hyperthermia Enhances the Anti-tumor Effects of Cisplatin and Adriamycin in Human Bladder Cancer T24 Cells In Vitro. *Experimental and Therapeutic Medicine* **2010**, 1, 319-323.
7. Li, X.; Lovell, J. F.; Yoon, J.; Chen, X. Clinical Development and Potential of Photothermal and Photodynamic Therapies for Cancer. *Nat. Rev. Clin. Oncol.* **2020**, 17, 657-674.
8. Hsiao, C. W.; Chuang, E. Y.; Chen, H. L.; Wan, D.; Korupalli, C.; Liao, Z. X.; Chiu, Y. L.; Chia, W. T.; Lin, K. J.; Sung, H. W. Photothermal Tumor Ablation in Mice with Repeated Therapy Sessions Using NIR-absorbing Micellar Hydrogels Formed In Situ. *Biomaterials* **2015**, 56, 26-35.
9. Ahn, G.-Y.; Choi, I.; Yun, T. H.; Choi, S.-W. Fabrication of Starch-Lauric Acid Nanoparticles for Potential Tumor Therapy. *Polym. Korea* **2021**, 45, 62-67.
10. Hwang, J.; Jin, J. O. Attachable Hydrogel Containing Indocyanine Green for Selective Photothermal Therapy against Melanoma. *Biomolecules* **2020**, 10, 1124.
11. Chu, Y.; Liao, S.; Liao, H.; Lu, Y.; Geng, X.; Wu, D.; Pei, J.; Wang, Y. Second Near-infrared Photothermal Therapy with Superior Penetrability Through Skin Tissues. *CCS. Chem.* **2022**, 4, 3002-3013.
12. Marshall, R. P.; Vlková, K. Spectral Dependence of Laser Light on Light-tissue Interactions and Its Influence on Laser Therapy: An Experimental Study. *Archivos De Medicina* **2020**, 5, 5.
13. He, Y.; Cao, Y.; Wang, Y. Progress on Photothermal Conversion in the Second NIR Window Based on Conjugated Polymers. *Asian J. Org. Chem.* **2018**, 7, 2201-2212.
14. Sun, R.; Chen, H.; Sutrisno, L.; Kawazoe, N.; Chen, G. Nanomaterials and Their Composite Scaffolds for Photothermal Therapy and Tissue Engineering Applications. *Sci. Technol. Adv. Mater.* **2021**, 22, 404-428.
15. Dai, X.; Li, X.; Liu, Y.; Yan, F. Recent Advances in Nanoparticles-based Photothermal Therapy Synergizing with Immune Checkpoint Blockade Therapy. *Mater. Design* **2022**, 110656.
16. Hwang, J.; An, E. K.; Kim, S. J.; Zhang, W.; Jin, J. O. Escherichia Coli Mimetic Gold Nanorod-Mediated Photo- and Immunotherapy for Treating Cancer and Its Metastasis. *ACS Nano.* **2022**, 16, 8472-8483.
17. Montaseri, H.; Kruger, C. A.; Abrahamse, H. Recent Advances in Porphyrin-Based Inorganic Nanoparticles for Cancer Treatment. *Int. J. Mol. Sci.* **2020**, 21, 3358.
18. Kim, M.; Noh, H. Study on Colloidal Stability of Gold Nanoparticles Modified with Sugar Molecules. *Polym. Korea* **2022**, 46, 68-73.
19. Zhao, L.; Zhang, X.; Wang, X.; Guan, X.; Zhang, W.; Ma, J. Recent Advances in Selective Photothermal Therapy of Tumor. *J. Nanobiotechnology* **2021**, 19, 335.
20. Hwang, J.; An, E. K.; Zhang, W.; Park, H. B.; Kim, S. J.; Yadav, D.; Kim, J.; Choi, I.; Kwak, M.; Lee, P. C.; Zhang, X.; Xu, J.; Jin, J. O. Recombinant Programmed Cell Death Protein 1 Functions as An Immune Check Point Blockade and Enhances Anti-cancer Immunity. *Biomaterials* **2022**, 285, 121550.
21. Kang, M.; Kim, H.; Lee, T. H.; Huh, Y. H.; Kim, Y. S.; Park, S. J.; Jin, J.-O.; Lee, P. C.; Kwak, M. Highly Photostable Rylene-encapsulated Polymeric Nanoparticles for Fluorescent Labeling in Biological System. *J. Ind. Eng. Chem.* **2019**, 80, 239-246.
22. Soeriawidjaja, B. F.; Kang, M.; Kim, H.; Yang, H. K.; Kim, J. H.; Kwak, M. Near Infrared Dye-encapsulated Polymeric Nanoparticles with Enhanced Photostability Under Hyperthermal Condition. *Molecular Crystals and Liquid Crystals* **2019**, 687, 53-59.
23. Cho, J.; Prasad, B.; Kim, J. K. Near-infrared Laser Irradiation of a Multilayer Agar-gel Tissue Phantom to Induce Thermal Effect of Traditional Moxibustion. *J. Innovative Optical Health Sci.* **2018**, 11, 1850033.
24. Vardaki, M. Z.; Kourkoumelis, N. Tissue Phantoms for Biomedical Applications in Raman Spectroscopy: A Review. *Biomed. Eng. Comput. Biol.* **2020**, 11, DOI: 10.1177/117959770948100.
25. Lai, P.; Xu, X.; Wang, L. V. Dependence of Optical Scattering From Intralipid in Gelatin-gel Based Tissue-mimicking Phantoms on Mixing Temperature and Time. *J. Biomed. Opt.* **2014**, 19, 35002.
26. Iizuka, M. N.; Sherar, M. D.; Vitkin, I. A. Optical Phantom Materials for Near Infrared Laser Photocoagulation Studies. *Lasers Surg. Med.* **1999**, 25, 159-69.
27. Geoghegan, R.; Santamaria, A.; Priester, A.; Zhang, L.; Wu, H.; Grundfest, W.; Marks, L.; Natarajan, S. A Tissue-mimicking Prostate Phantom for 980 nm Laser Interstitial Thermal Therapy. *Int. J. Hyperthermia* **2019**, 36, 993-1002.
28. Ashrafi, S. J.; Yazdian, F.; Zaremi, A. S. H.; Mohhamadnejad, J.; Dinarvand, R. Thermal Distribution of Silica Coated Gold Nano Rods in Tissue-Like Phantom as In Vitro Model for Plasmonic Photo Thermal Therapy. *Biomed. Pharmacol. J.* **2016**, 9, 1189-1201.
29. Bini, M. G.; Ignesti, A.; Millanta, L.; Olmi, R.; Rubino, N.; Vanni, R. The Polyacrylamide as a Phantom Material for Electromagnetic Hyperthermia Studies. *IEEE Trans Biomed Eng* **1984**, 31, 317-22.
30. Pogue, B. W.; Patterson, M. S. Review of Tissue Simulating Phantoms for Optical Spectroscopy, Imaging and Dosimetry. *J. Biomed. Opt.* **2006**, 11, 041102.
31. Lepore, M.; Delfino, I. Intralipid-based Phantoms for the Development of New Optical Diagnostic Techniques. *Open. Biotechnol. J.* **2019**, 13, 163-172.
32. Flock, S. T.; Jacques, S. L.; Wilson, B. C.; Star, W. M.; van Gemert, M. J. Optical Properties of Intralipid: a Phantom Medium for Light Propagation Studies. *Lasers Surg. Med.* **1992**, 12, 510-519.
33. Asadi, S.; Korganbayev, S.; Xu, W.; Mapanao, A. K.; Voliani, V.;

Lehto, V. P.; Saccomandi, P. Experimental Evaluation of Radiation Response and Thermal Properties of NPs-Loaded Tissues-Mimicking Phantoms. *Nanomaterials (Basel)* **2022**, 12, 945.
34. Nourhashemi, M.; Mahmoudzadeh, M.; Wallois, F. Thermal Impact of Near-infrared Laser in Advanced Noninvasive Optical Brain Imaging. *Neurophotonics* **2016**, 3, 015001.
35. Pradyasti, A.; Kim, D. S.; Kim, M. H. Synthesis of Au@AgAuS Core–shell Hybrid Nanorods and Their Photocatalytic Application. *Colloid and Interface Sci. Commun.* **2022**, 49, 100635.
36. Pradyasti, A.; Hoang, H. T.; Lim, K. T.; Kim, M. H. Synthesis of Porous Ag–Ag2S@ Ag–Au Hybrid Nanostructures with Broadband Absorption Properties and Their Photothermal Conversion Application. *J. Alloys Compos.* **2022**, 896, 163062.
37. Choi, H.; Soeriawidjaja, B. F.; Lee, S. H.; Kwak, M. A Convenient Platform for Real-time Non-contact Thermal Measurement and Processing. *Bull. Korean Chem. Soc.* **2022**, 43, 854-858.
38. Zhao, X.; Zhao, H.; Wang, S.; Fan, Z.; Ma, Y.; Yin, Y.; Wang, W.; Xi, R.; Meng, M. A Tumor-Targeting Near-Infrared Heptamethine Cyanine Photosensitizer with Twisted Molecular Structure for Enhanced Imaging-Guided Cancer Phototherapy. *J. Am. Chem. Soc.* **2021**, 143, 20828-20836.
39. Nejabat, M.; Samie, A.; Ramezani, M.; Alibolandi, M.; Abnous, K.; Taghdisi, S. M. An Overview on Gold Nanorods as Versatile Nanoparticles in Cancer Therapy. *J. Control. Release* **2023**, 354, 221-242.